Journal of Asian Earth Sciences 98 (2015) 50–60

Contents lists available at ScienceDirect

Journal of Asian Earth Sciences

journal homepage: www.elsevier.com/locate/jseaes

Frequent excitations of *T* waves by earthquakes in the South Mariana Arc

Po-Fei Chen *, Kai-Xun Chen, Hui-Yun Cheng

Department of Earth Sciences, National Central University, Taiwan

ARTICLE INFO

Article history:
Received 6 June 2014
Received in revised form 22 September 2014
Accepted 15 October 2014
Available online 7 November 2014

Keywords:
T wave
South Mariana Arc
Broadband in Taiwan for Seismology
F-net

ABSTRACT

We used broadband stations in Taiwan and on the Ryukyu Arc islands to investigate *T* waves induced by earthquakes in the Izu-Bonin-Mariana subduction zone. Of the 48 earthquakes that took place in 2005, 17 earthquakes exhibited *T*-wave signals consistent with predicted arrival times at stations. Of theses *T*-excited events, 13 were located in the South Mariana Arc, where the isobaths exhibit strong concave curvature, and were predominantly of normal faulting type. The energies of observed *T* waves were used quantitatively to evaluate the relative efficiency of receiver-side acoustic–elastic conversions by Gamma calculations. Results show that the steep slopes of offshore bathymetry together with nearly perpendicular angles of back azimuth relative to local isobaths are suitable conditions for *T* waves observations. In 2010, two clusters of repeated moderate earthquakes in the north and south ends of the Mariana Arc displayed stark contrasts in terms of *T*-wave excitations despite their normal faulting type. Examining of this discrepancy indicate that a specific curvature together with a specific radiation pattern accounts for the frequent excitations of *T* waves from shallow earthquakes in the South Mariana Arc.

1. Introduction

T waves refer to seismic energies trapped within and efficiently propagating through the Sound Fixing and Ranging (SOFAR) (Ewing et al., 1946) channel of an ocean that are distinguished as the Tertiary phase on seismograms, following Primary (*P* wave) and Secondary (*S* wave) phases (Linehan, 1940). *T* waves on seismograms exhibit spindle-shape envelope of frequency contents greater than 2.5 Hz with group velocities at ca. 1.5 km/s (Okal, 2008), and characteristics of weak dispersion due to variation in Fresnel zone widths resulting slightly varying mean velocities over ocean column of the SOFAR (Park et al., 2001). The fact that propagation paths and the resulting *T* waveforms starkly contrast with those of body waves has provided alternative approaches for seismic studies: (1) Talandier and Okal (2001) discriminate between explosive sources in the water column and elastic dislocations in solid earth using the maximum amplitude and duration of the *T* waves envelope. (2) Observations of *T* waves converted from *S* waves of the 1994 Bolivian deep earthquake favor the attribution of the seismic gap 300–600 km beneath Southern Peru (Chen et al., 2004) to continuity of an aseismic slab (Okal and Talandier, 1997). (3) Propagation through 2-D SOFAR without substantial energy loss allows *T* waves to be used for detecting and locating small seismic events (e.g., Duennebier and Johnson, 1967; Walker, 1989).

However, *T* waves are not initiated by all earthquakes, and both the source and receiver sides require suitable conditions for elastic–acoustic and acoustic–elastic conversions, respectively. Regarding the source-side, two main mechanisms have been proposed to explain apparently suitable conditions for elastic–acoustic conversions: downslope conversion (Johnson et al., 1963; Talandier and Okal, 1998) and seafloor scattering (deGroot-Hedlin and Orcutt, 1999). Downslope conversion is a geometrical ray illumination of the penetration of energy into the SOFAR channel by progressively decreasing incident angles as waves bounce back and forth between sea surface and sloping sea floor. While this approach fails to explain the excitation of the abyssal *T* phase, modal propagation has been put forward to explain the energy trapped in SOFAR originating from broadband scattering by a rough seafloor (Okal, 2008). Other case-specific factors have also been proposed. The empirical relationships for northeast Pacific Ocean earthquakes indicate that the *T* wave energy at the seafloor–ocean interface is higher for strike-slip events than for normal/reverse fault events of the same seismic magnitude (Dziak, 2001). The concave isobaths at the Arica Bight and the Hokkaido corner are attributable to the conversion of *T* waves from the seismic waves of the great 1994 Bolivian deep earthquake (Okal and Talandier, 1997) and of the 1994 deep earthquake under the Primorye province of Eastern Russia (Okal, 2001), respectively.

With respect to the receiver side, the acoustic–elastic conversions are intuitively straightforward and no mechanisms need be proposed. Talandier and Okal (1998) underlined that steeply

* Corresponding author. Tel.: +886 3 4227151 65647.
E-mail address: bob@ncu.edu.tw (P.-F. Chen).

http://dx.doi.org/10.1016/j.jseaes.2014.10.033
1367-9120/

Table 1
List of the GCMT parameters for earthquakes studied. Those with observed *T* phase are marked with asterisk. M_1, M_2, and M_3 multiplied by 10 to the exp. are eigenvalues expressed in principal-axis system. ε is a measure of non-double couple component.

Event No.	Date	Origin time	Long.(°)	Lat.(°)	Depth(km)	M_0(dyn-cm)	M_w	M_1	M_2	M_3	exp.	ε
1*	1/16/2005	20:17:52.8	140.84	10.93	25	1.00E+26	6.6	2.63	-0.08	-2.55	26	-0.03
2*	1/17/2005	10:50:32.6	140.68	10.99	12	1.50E+25	6.1	4.9	-0.66	-4.24	25	-0.13
3	1/19/2005	6:11:36.4	141.49	34.06	28	8.10E+25	6.5	9.96	1.87	-11.83	25	0.16
4	1/20/2005	14:16:26.8	141.51	33.86	51	1.30E+24	5.3	1.31	0.38	-1.7	24	0.22
5	1/21/2005	12:45:31.5	141.55	34.02	10	2.60E+24	5.5	15.71	-3.68	-12.03	24	-0.23
6	1/21/2005	17:58:56.4	141.37	34	10	4.00E+24	5.7	1.76	0.76	-2.52	24	0.3
7	1/27/2005	3:56:42.8	140.44	27.22	175	6.70E+23	5.2	7.64	0.63	-8.27	24	0.08
8*	2/2/2005	2:30:25.9	144.71	14.08	159	3.10E+25	6.3	2.9	0.29	-3.19	25	0.09
9	2/4/2005	16:06:28.8	145.45	17.52	512	1.20E+24	5.3	1.348	-0.199	-1.146	24	-0.15
10*	2/5/2005	3:34:25.7	145.87	16.01	143	9.00E+25	6.6	9.9	0.41	-10.3	26	0.04
11*	2/9/2005	18:46:10.0	144	26.09	24	3.10E+25	6.3	4.49	0.63	-5.12	25	0.12
12	2/22/2005	11:20:25.3	137.15	33.18	370	3.30E+24	5.6	2.07	-0.28	-1.8	24	-0.14
13	4/19/2005	1:46:57.0	138.89	29.64	426	8.30E+24	5.9	4.91	0.53	-5.45	24	0.1
14*	4/21/2005	21:31:48.8	145.06	13.18	50	1.50E+24	5.4	7.2	0.08	-7.28	24	0.01
15	5/4/2005	4:38:06.6	143.78	11.71	10	1.30E+24	5.3	1.91	-0.37	-1.54	24	-0.19
16	5/21/2005	16:29:22.7	138.46	30.71	396	6.40E+23	5.1	3.72	0.25	-3.97	23	0.06
17	5/28/2005	20:55:12.0	137.55	34.4	296	8.00E+23	5.2	2.54	0.18	-2.72	24	0.07
18*	5/29/2005	3:32:31.3	144.92	16.21	10	2.00E+24	5.5	4.4	-0.34	-4.05	24	-0.08
19	5/30/2005	11:18:10.9	140.79	31.92	62	6.40E+23	5.1	3.41	-0.39	-3.02	23	-0.11
20	6/15/2005	15:01:46.3	144.37	22.84	81	1.00E+24	5.3	1.054	-0.047	-1.006	24	-0.04
21	7/1/2005	9:36:16.4	139.06	31.92	206	2.20E+24	5.5	3.77	0.24	-4	24	0.06
22	7/9/2005	23:37:11.1	140.82	33.42	55	5.70E+24	5.8	2.57	0.17	-2.74	24	0.06
23	7/27/2005	2:39:22.6	142.32	33.26	34	9.00E+23	5.2	9.29	0.18	-9.47	24	0.02
24	7/27/2005	15:51:38.4	142.43	33.25	34	5.20E+23	5.1	2.32	-0.43	-1.89	23	-0.19
25	7/29/2005	12:51:06.6	142.43	33.25	36	7.30E+23	5.2	5.21	-1.21	-4	23	-0.23
26	7/29/2005	20:25:00.1	142.36	33.32	11	1.50E+24	5.4	2.1	-0.72	-1.38	24	-0.34
27	8/10/2005	15:10:49.2	145.52	16.75	26	1.50E+24	5.4	1.98	0.01	-1.98	24	0.01
28*	8/13/2005	7:36:52.8	145.8	20.13	49	1.20E+25	6	8.96	-1.21	-7.74	25	-0.14
29	8/16/2005	19:15:34.2	140.76	31.93	62	5.60E+23	5.1	2.18	-0.05	-2.13	23	-0.02
30	8/31/2005	16:29:42.3	138.42	10.3	11	1.40E+24	5.4	3.72	0.25	-3.97	24	0.06
31*	9/1/2005	23:36:55.1	138.43	10.37	10	8.00E+23	5.2	14.1	-1.14	-12.96	24	-0.08
32*	9/2/2005	18:35:12.7	138.32	10.36	10	4.10E+24	5.7	2.47	0.53	-3	24	0.18
33	9/24/2005	14:48:48.3	140.82	34.3	66	7.00E+23	5.2	2.69	-0.23	-2.46	24	-0.09
34	10/4/2005	4:33:44.9	145.12	18.85	490	7.60E+23	5.2	1	0.64	-1.64	23	0.39
35	10/27/2005	8:41:46.8	138.47	30.87	382	6.80E+23	5.2	1.62	0.09	-1.72	23	0.05
36	11/15/2005	20:20:45.8	141.35	33.34	16	4.90E+24	5.7	7.2	2.07	-9.27	24	0.22
37	11/15/2005	23:1:10.1	144.8	22.04	20	5.30E+24	5.8	5.172	0.178	-5.348	24	0.03
38	11/16/2005	23:48:35.8	142.21	23.32	50	6.00E+23	5.1	1.49	-0.15	-1.34	23	-0.1
39	11/17/2005	21:59:29.9	141.39	33.32	10	3.90E+24	5.7	3.4	-0.46	-2.94	24	-0.14
40*	11/28/2005	16:41:32.5	146.04	20.29	41	1.20E+25	6	5.87	-0.23	-5.64	25	-0.04
41*	12/3/2005	20:38:11.9	141.01	12.19	10	3.90E+24	5.7	2.05	0.46	-2.5	24	0.18
42*	12/18/2005	4:29:16.0	141	12.22	28	6.90E+23	5.2	2.12	0.88	-3	23	0.29
43*	12/20/2005	5:51:12.6	140.99	12.23	23	1.90E+25	6.1	1.75	0.19	-1.95	25	0.1
44*	12/20/2005	16:5:40.7	140.94	12.24	29	1.10E+24	5.3	1.046	0.064	-1.11	24	0.06
45	12/23/2005	21:32:13.8	146.42	12.93	32	5.00E+23	5.1	4.91	0.38	-5.29	23	0.07
46*	12/26/2005	13:48:01.8	140.65	26.82	7	2.70E+24	5.6	13.78	2.38	-16.17	24	0.15
47*	12/26/2005	14:39:59.6	140.95	12.15	53	6.50E+23	5.1	3.56	-0.82	-2.74	23	-0.23
48	12/29/2005	8:30:34.5	139.85	27.37	472	1.10E+24	5.3	2.18	0.38	-2.55	24	0.15

sloping (typically 50°) of offshore bathymetry is particularly efficient for such conversions, using *T* waves of marine sources as observed across the Polynesian Islands. Accordingly, the *T* waves generated by a M6.8 earthquake in NE Japan, propagating reversely as scattered from the Emperor seamount chain, were detectable by Hi-net stations along the shoreline of NE Japan (Obara and Maeda, 2009). Kosuga (2011), using observations by a dense seismic network in NE Japan of these *T* waves, further investigated their terrestrial propagation characteristics and concluded that they constituted multiple arrivals of Rayleigh waves, non-isotropic radiation converted to the NE of Honshu Island, and had a predominant frequency of 1.5 Hz (slightly lower than typical values). Similarly, the steeply dipping bathymetry off Eastern Taiwan has resulted in frequent observations of *T* waves by either the early analog seismic network (Huang et al., 2011) or short period stations (Lin, 2001), which allows examinations of corresponding *T* wave propagation paths. In this study, we investigate scenarios of *T* wave generation by earthquakes in the Izu-Bonin-Mariana (IBM) subduction system using data from the Broadband Array in Taiwan for Seismology (BATS) (Kao et al., 1998) and broadband stations on the island chain of the Ryukyu Arc from F-net. This is based on the assumption that the coastlines of these stations are well positioned for receiver-side conversions and that any *T* waves initiated by the IBM events that propagate in the oceans of the Western Pacific can thus be observed. The purpose of the investigation was two fold: (1) By determining whether or not *T* waves are excited by earthquakes along the Izu-Bonin-Mariana trench, we infer the preferable source scenarios for *T* wave excitation and correlate previously proposed case-specific factors such as curvature of isobaths and types of earthquake focal mechanisms. (2) Using the *T* waves observed at different stations and calculating the corresponding elastic energies, we assess the preferable conditions for receiver-side acoustic–elastic conversions and correlate with factors such as seafloor slopes, inland distances, and angles of back azimuth relative to local isobaths.

2. Data and methods

We used the Global Centroid Moment Tensor (GCMT) catalog (Dziewonski et al., 1981; Ekström et al., 2005) to extract data on

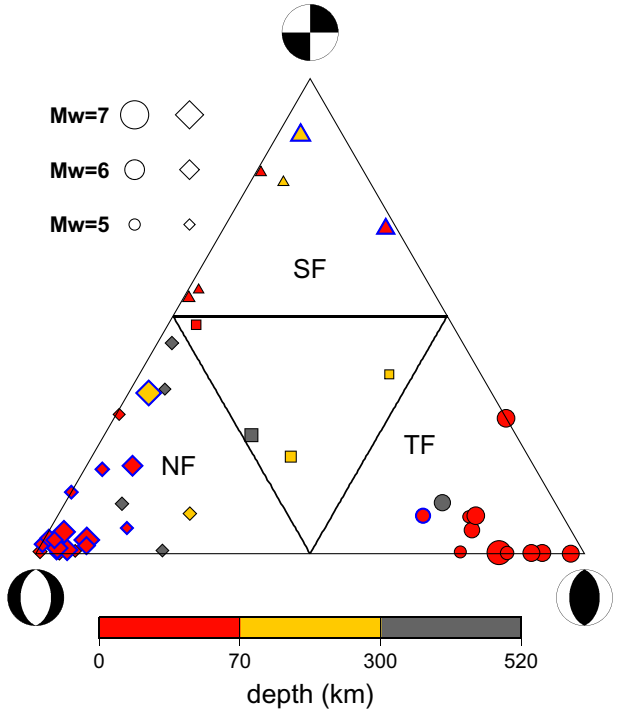

Fig. 1. Ternary diagram for display of earthquake focal mechanisms with $\log_{10}$ of moment gray-keyed. The three apexes indicate a pure strike-slip (top), a pure normal fault with 45° dipping plane (left), and a pure reverse fault with 45° dipping plane (right). The three solid lines inside the ternary represent **N** (top), **P** (left), **T** (right) axes of earthquakes being 45° from the vertical, respectively, which are the boundaries used to define the strike-slip fault (**SF**) group (triangles), the normal fault (**NF**) group (diamonds), the thrust fault (**TF**) group (circles), and others (squares). *T*-excited events are encircled with a blue line and mostly associated with normal faulting earthquakes in this study. (For interpretation of the references to colour in this figure legend, the reader is referred to the web version of this article.)

earthquakes that occurred in 2005, were bounded by 135°E/150°E and 5°S/35°N (IBM subduction zone), and had moments greater than 5.0×10^{23} dyn-cm. Table 1 lists the GCMT parameters of these earthquakes. Based on the double-couple components of focal mechanisms, the **P**, **N**, and **T** axes of compiled earthquakes were calculated and categorized into normal, strike-slip, and thrust types according to the angles between the vertical and the three axes, respectively. The categorization was carried out by a ternary diagram (Fig. 1) with a pure normal (vertical **P** axis), pure strike-slip (vertical **N** axis), and pure thrust (vertical **T** axis) event as end members (Frohlich and Apperson, 1992). An event with an angle of less than 45° between the vertical and **P** axis is projected near the corner of the pure normal end-member and is categorized as normal faulting (**NF,** indicated by diamonds in Fig. 1). Strike-slip faulting (**SF**, triangles) and thrust faulting (**TF**, circles) are similarly grouped by angles between the vertical and **N,** and vertical and **T** axis, respectively. Events projected in the middle sub-triangle of the ternary diagram are those with all three angles between the vertical and **P**, **N**, **T** axes greater than 45° and are not grouped into the above categories (squares in Fig. 1). The spatial distributions of earthquakes in each group were examined by plotting corresponding symbols on epicenters with sizes scaled to magnitude and depths color-coded (Fig. 2).

Next, seismic data from stations in and around Taiwan from BATS and on Ryukyu Arc islands from F-net were downloaded from the website to examine signals of *T* waves (Fig. 2). Instrument responses of vertical component seismograms were deconvolved to retrieve displacement waveforms, and a 2.0–8.0 Hz bandpass filter was applied. The predicted arrival times of *T* waves were derived by dividing the epicentral distances by 1.5 km/s and the time window 300 s before and after the predicted arrival were examined for potential signals of *T* waves. Ratios of short-term average (20 s) over long-term average (400 s) were calculated. Data without ratios exceeding a threshold value (1.5) within the time window were discarded. Remaining data, were then visually inspected for *T*-wave association based on three criteria: (1) whether signals were in the neighborhood of predicted arrival times; (2) whether signals exhibited the typical spindle-shape envelope of *T* waves and had suitable frequency contents in spectrograms; (3) whether 1 and 2 were consistently observed across several stations of the employed network. Earthquakes complying with all three criteria were considered to be *T*-excited events (Figs. 3 and 4), and marked with an asterisk after the event number in Table 1 and with solid blue outlines in Figs. 1 and 2.

The varying *T* wave energies of a *T*-excited earthquake between stations (or the absence of *T* waves) were used to assess the efficiency of receiver-side conversions. Stations were grouped into four categories based on location proximity and distance to the coastline. Resulting observations of *T* waves are shown in Fig. 5. Group 1 comprises stations on Ryukyu Arc islands; Group 2, stations near the Eastern Taiwan coastlines and LYU on Lanyu Island; Group 3, stations further inland near the Central Mountain Range; Group 4, stations in Western Taiwan and on Taiwan Strait islands. For groups with *T* wave observations (Groups 1, 2, and 3), the *T*-phase efficiencies (γ) are calculated as follows (Okal et al., 2003):

$$\gamma = \frac{TPEF}{M_0} = \frac{\rho\alpha \int_{t_1}^{t_2} [\dot{u}(t)]^2 dt}{M_0}, \quad (1)$$

where γ represents the *T*-phase energy flux (*TPEF*) normalized by the moment (M_0) of the earthquake. *TPEF* in turn is calculated by integrating the square of filtered vertical ground velocity ($\dot{u}(t)$) over a suitable time window (t_1–t_2) encompassing *T* waves and multiplying by density (ρ) and the *P*-wave velocity (α) of the shallow velocity structure (Boatwright and Choy, 1986). ρ and α are taken as 2600 kg/m^3 and 5.8 km/s (values typical of crusts). The filtered band for *T* wave calculations is 2–10 Hz. An appropriate time window to include energies of *T* wave was chosen for calculations of Gamma (γ). Fig. 6 shows the positive correlations between *T* amplitudes and γ. For each station, Gamma values for those events with observed *T* waves among all *T*-excited events were summed and this value divided by the number of observed *T* waves for that station, yielding the mean Gamma values. Fig. 7 shows average Gamma values of each station in Groups 1–3, ordered and numbered counter-clockwise, together with standard deviation and number of observed *T* waves.

3. Results

Although the IBM subduction zone is located on the convergent boundary between the Pacific and Philippine Sea Plates, the main rupture types for prevailing shallow earthquakes in this region are **TF** and **NF** types dominant in number and size, with only a few **SF** type minor-sized earthquakes (Fig. 1). Examination of the spatial distributions of each type of earthquake reveals that **TF** type earthquakes represent interplate earthquakes that occurred in the Izu-Bonin trench, whereas **NF** type earthquakes are associated with back-arc spreading earthquakes in the Mariana trench (Fig. 2). It is interesting to note that the latter appears to have a higher tendency to be a *T* wave excited event (Fig. 2). A total of 17 of the 48 earthquakes examined in this study were *T*-excited (Table 1), with the majority being **NF** type shallow earthquakes located at the southernmost termination of the Mariana trench. The conditions for *T* generation are so consistent here that

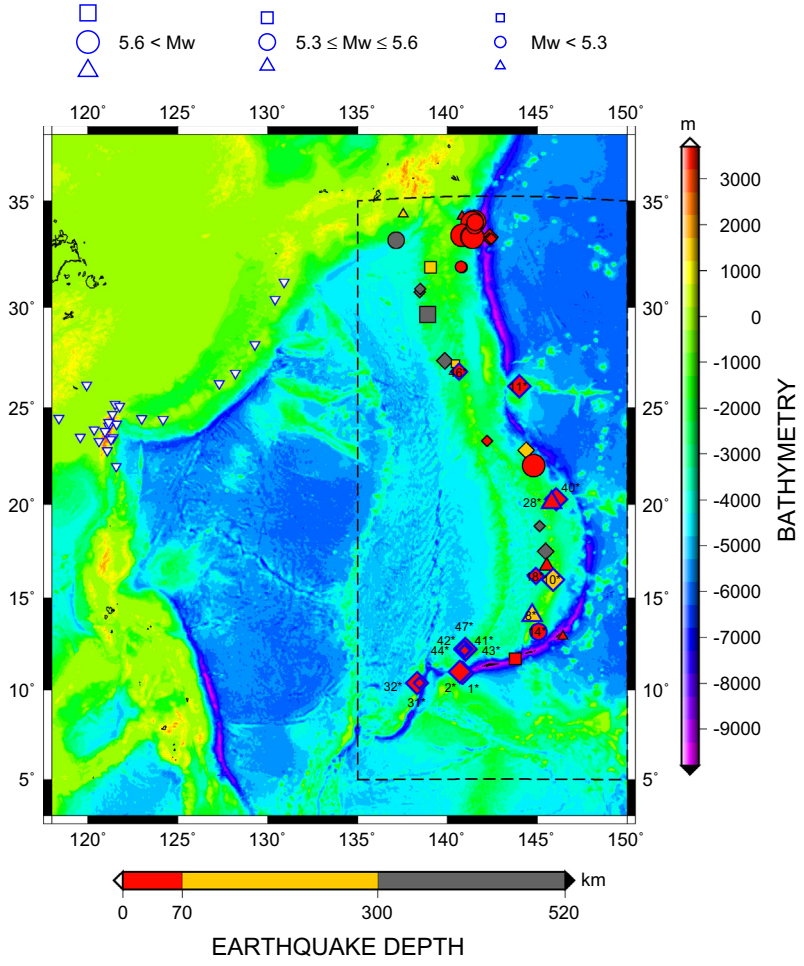

Fig. 2. Distributions of earthquakes in the Izu-Bonin-Mariana subduction zone (bounded by dashed box) in 2005 and stations (reversed triangles) for *T* wave observations in Taiwan and the Ryukyu Arc islands. Different symbols (triangles for **SF**, diamonds for **NF**, circles for **TF**, and squares for others) are used to indicate different types of earthquake ruptures following those of Fig. 1 with sizes proportional to earthquake magnitudes (scales on top) and depths gray-keyed. *T*-excited events are outlined in blue and event numbers (Table 1) are indicated. Note that earthquakes in the South Mariana Arc are predominantly **NF** type earthquakes and *T*-excited.

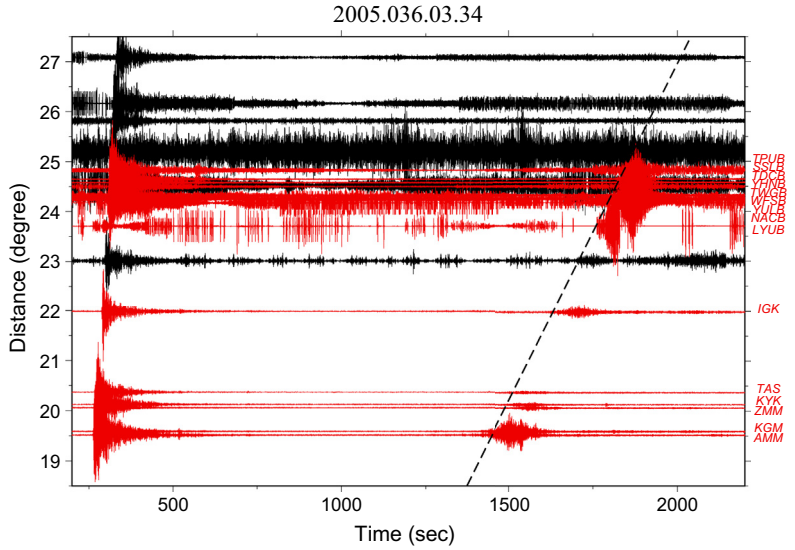

Fig. 3. Example record of a *T*-excited event with time (sec) relative to origin time of earthquake on the *x*-axis and epicentral distance in degrees on the *y*-axis. The slope line is indicative of theoretical T arrival time, calculated from epicentral distances divided by 1.5 (km/s). Note the consistent spindle-like signals in several stations (in red with station name labeled) in the vicinity of the predicted arrival time. For comparison, those without observed *T*-waves are shown in black. Earthquake depth was 134 km (10* in Table 1). Numbers on top indicate the origin time of this earthquake (year, Julian day, hour, minute). (For interpretation of the references to colour in this figure legend, the reader is referred to the web version of this article.)

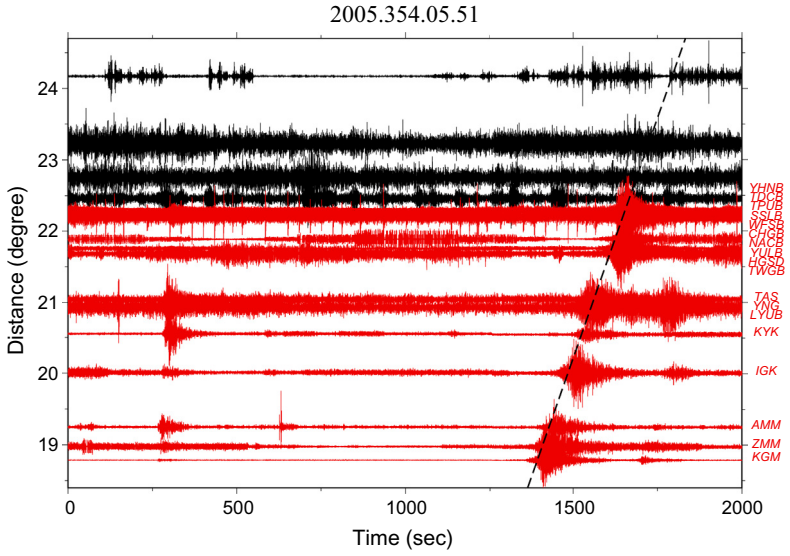

Fig. 4. As per Fig. 3 but for a shallow earthquake (43* in Table 1).

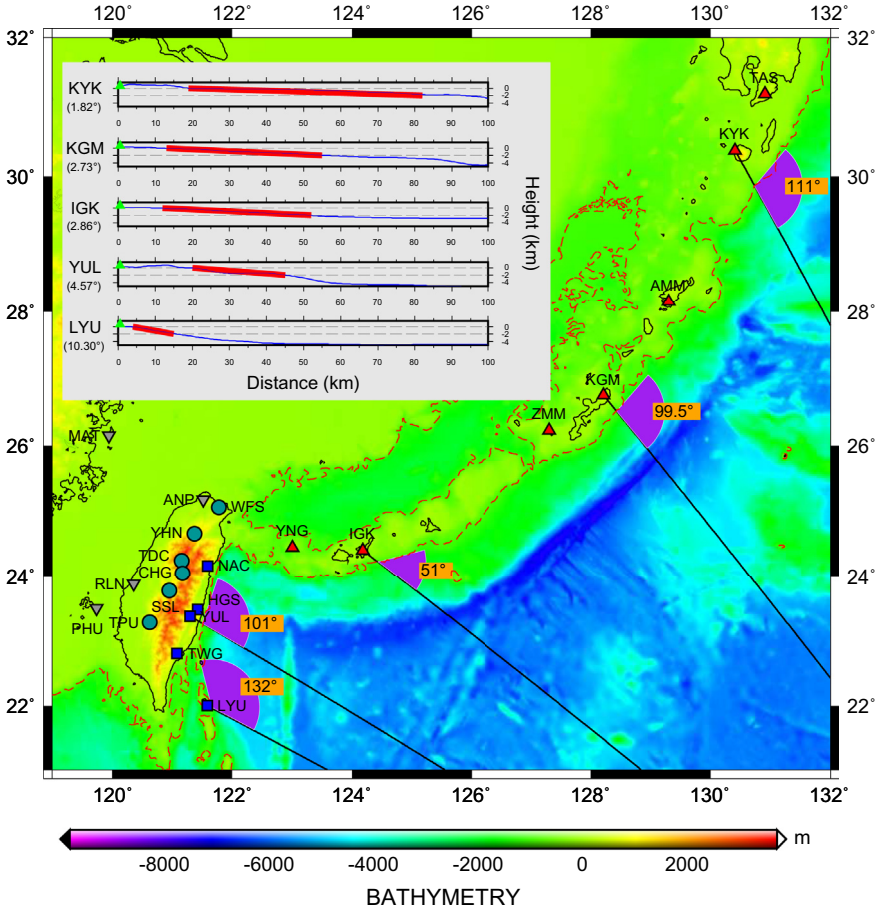

Fig. 5. Distribution of observation stations. The stations are divided into four groups represented by different symbols. Group 1: Ryukyu Arc islands (triangles); Group 2: Eastern Taiwan coastline and Orchid (Lanyu) island (squares); Group 3: along the NS line of the Central Mountain Range (circles); Group 4: Western Taiwan and Taiwan Strait islands (reverse triangles). Red dashed lines: 1000 m isobaths. Five stations are selected to show the great circle paths of earthquakes in the South Mariana Arc (black solid lines), the back azimuth relative to local isobaths (BAI angles, purple fans), and the slopes of bathymetry (inlet with red lines showing fitting of bathymetry and slopes indicated). (For interpretation of the references to colour in this figure legend, the reader is referred to the web version of this article.)

earthquakes with M_w as small as 5.1 could be *T*-excited events (37* and 41* in Table 1). Other *T*-excited events not belonging to this category possess at least one of the following characteristics: (1) **NF** type (10*, 11*, 18*, 40*), (2) locations on the southern half of the Mariana Arc (8*, 14*), (3) M_w no less than 6.0 (28*). However, earthquakes fulfilling one of these three conditions but that were

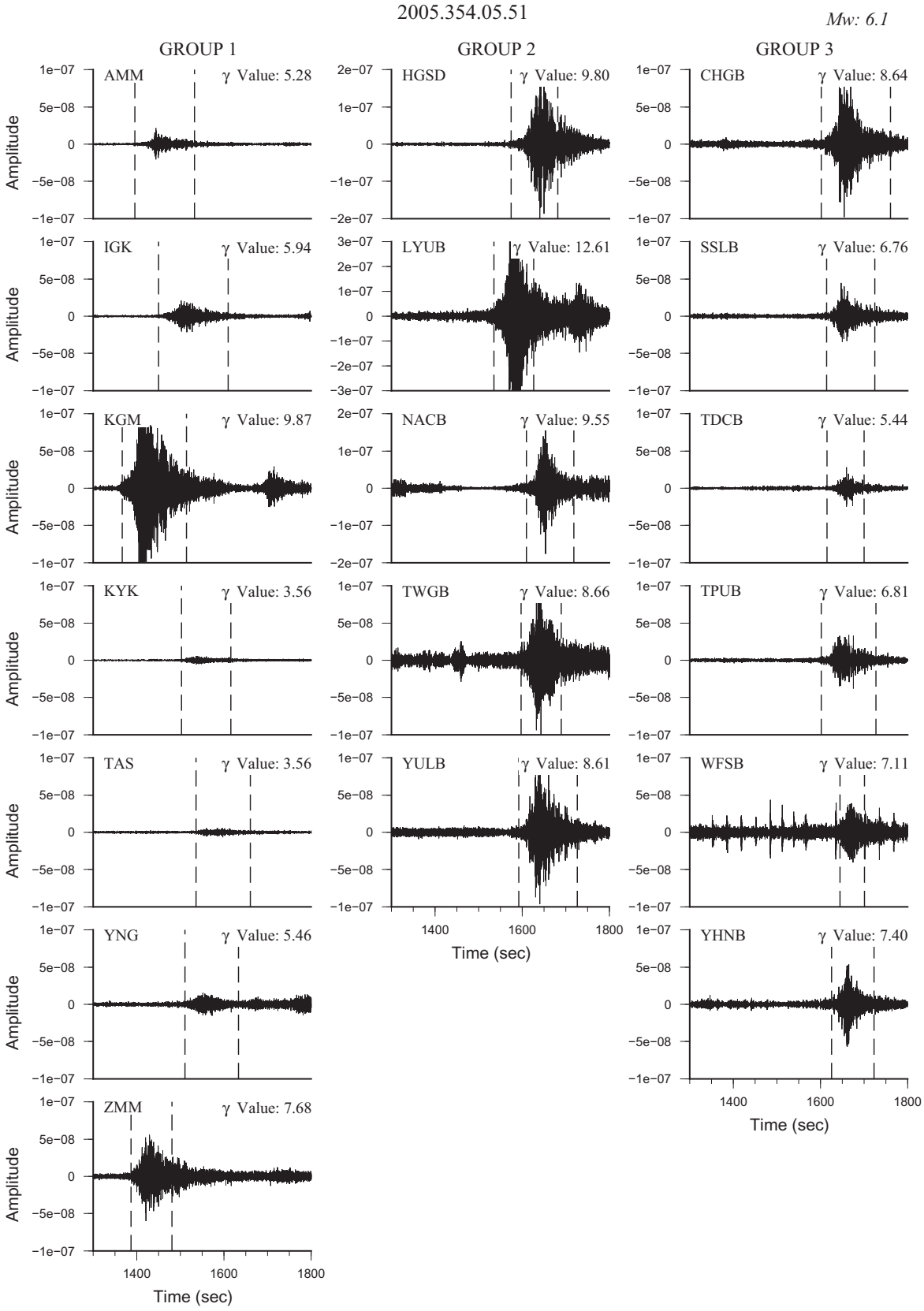

Fig. 6. Time windows (vertical dashed lines) to include *T* waves and calculated Gamma (γ) values for the example earthquake shown in Fig. 4 arranged by Groups of stations. Note the high γ of Group 2 stations where the scale of the *y*-axis is doubled for HGSD, NACB and tripled for LYUB.

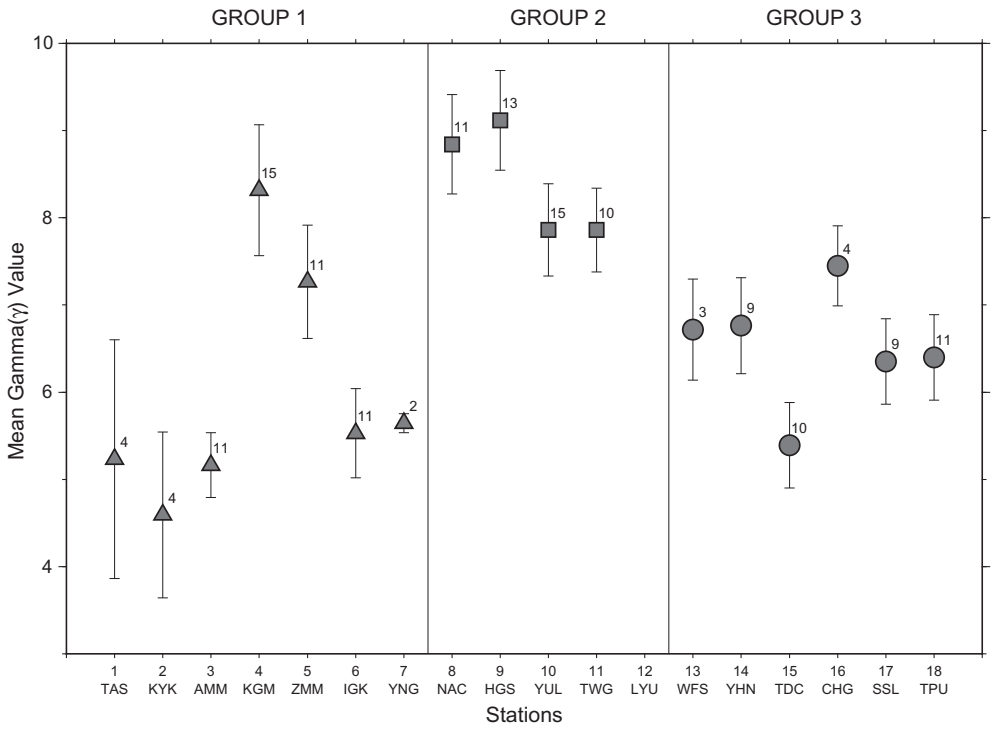

Fig. 7. Mean Gamma values of stations arranged in order from Groups 1 to Group 3. See Fig. 5 for the locations of stations. The numbers attached to each data point are the numbers of *T*-wave observations at each station, while their mean and standard deviation are shown as position and length on the *y*-axis, respectively.

not *T*-excited were also consistently found. In other words, no single condition alone is decisive for *T* excitation.

The observed amounts of *T* wave energies of one earthquake varied between stations depending on the receiver-side conditions for acoustic–elastic conversions. Firstly, stations in Western Taiwan (Group 4) were the least likely to observe *T* waves in any case of significant attenuation and 3-D geometrical spreading of energies propagating in solid media. Secondly, stations in the Central Mountain Range (Group 3) tended to observe *T* waves of *T*-excited earthquakes (Fig. 7), suggesting that 100 km landward is probably the threshold distance for observing the elastic energies converted along the Eastern Taiwan coastlines. Thirdly, Eastern Taiwan coastline stations and LYU (Group 2) recorded the highest overall mean Gamma values and the highest numbers of *T* wave observations, reinforcing the important role of steeply sloping offshore bathymetry in receiver-side conversions (Talandier and Okal, 1998) and justifying our assumption that Eastern Taiwan coastlines are well positioned for conversions. Note that while Lanyu Island station (LYU) was the station with the highest observed mean Gamma value (Fig. 7), only nine *T* wave observations were recorded here due intermittent instrumental failure.

Finally, stations on the Ryukyu Arc islands (Group 1) exhibited overall mean Gamma values that were slightly below those of Group 3 and had an overall convex upward shape with maximum at the center (KGM) (Fig. 7). It is counterintuitive that *T* wave energies of island stations should be lower than those of inland stations, given similar epicentral distances. These results are attributable to two different conditions: the slope of offshore bathymetry and back azimuth relative to local isobaths (BAI angle). Average slopes for stations on the Ryukyu Arc islands, Eastern Taiwan coastline, and Lanyu Island are approximately 2°, 5°, and 10°, respectively (Fig. 5). Ray geometry was used to illustrate that the minor differences in slopes are significant in controlling the efficiency of receiver-side conversions. The BAI angles drawn for one earthquake are representative of others mostly because *T*-excited earthquakes are spatially clustering. The pattern of BAI angle variations, with the one of KGM closest to 90° and increasing obliquity for stations on both sides (Fig. 5), is consistent with upward distributions of Gamma values (Fig. 7) and suggests that near perpendicular BAI angles are also a factor in the efficiency of receiver-side conversions. Kosuga (2011) points out that the maximum amplitude of acoustic–elastic converted energy is expected to appear in either the propagation direction of incoming acoustic waves or the steepest direction of the local topography. A perpendicular BAI angle complies with both conditions.

4. Discussion

One of the main findings of this study is the exceptionally high probability of *T* wave excitation in the cluster of shallow earthquakes at the southernmost termination of the Mariana trench (Fig. 2). Almost all of these earthquakes are of **NF** type on a trench with strong concave geometry. We cannot determine whether **NF** type of earthquake or concave trench is the critical factor in *T* wave excitation. If the excitation was dominated by **NF** type of earthquake, this contradicts the proposal by Dziak (2001) who suggested that the **SF** type was dominant in *T* wave excitation and the observations that other types of earthquakes also excited *T* wave in this study (8*, 14*, 40*). If the concave trench is the critical factor, as supported by the observations of Okal and Talandier (1997) and Okal (2001), the lack of theoretical foundation also cannot rule out the possibility of divergent interpretations. The non-double component of earthquakes was investigated (last column of Table 1) but no correlation was found with excitations of *T* waves, thus this factor was ruled out.

In August and December 2010, two series of repeated shallow earthquakes (mostly $M_w > 4.5$) occurred with the earlier one clustering exactly at the southernmost termination of the Mariana trench (South Series) and the latter one at the southernmost termination of the Bonin trench (North Series) (Figs. 8 and 9). Earthquakes within each cluster exhibited focal mechanisms resembling the **NF** type, but the orientation of faulting was

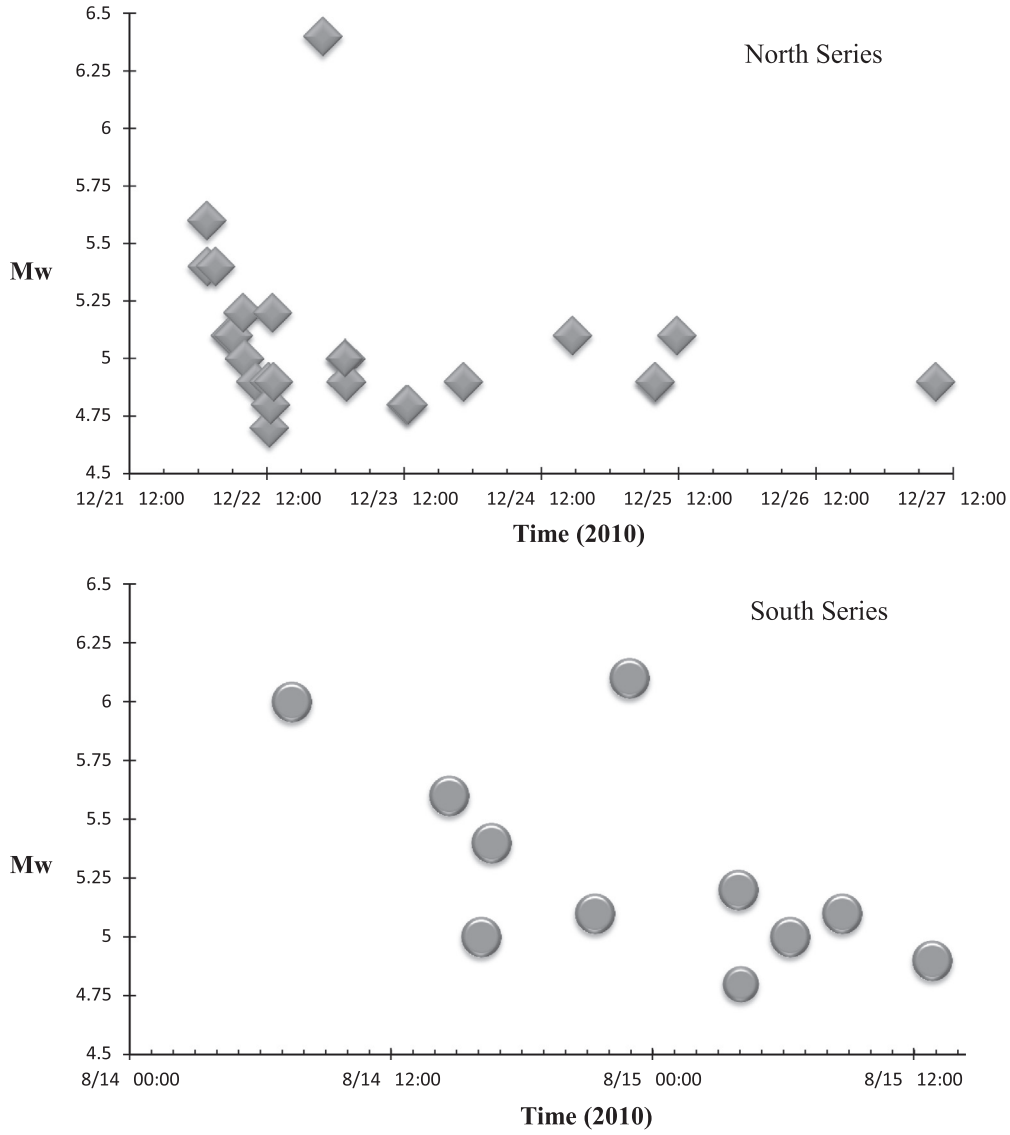

Fig. 8. Moment magnitudes (M_w) as a function of time for the two moderate earthquake series in 2010 (see Fig. 9 for locations). Note the fore-, main-, and after-shock series for the North series, where more than 20 events occurred within five days in December. In August more than ten moderate earthquakes occurred within two days.

different between clusters. Examination of the associated *T* waves of these earthquakes shows that the two clusters exhibit starkly contrasting results in terms of *T* excitation – all earthquakes from the South Series were *T*-excited except for one M_w 5.1 event and all earthquakes from the North Series were not *T*-excited except for one M_w 6.4 event. A preliminary conclusion is that **NF** type is not a key factor here, but the role of concave trench remains to be determined. To investigate the relationships between *P* and *SV* wave radiation patterns and *T* excitation, we plotted typical earthquakes of the North and South Series and marked the poles of take-off for *P* waves to stations (Fig. 10), using lower-hemispherical projection (Herrmann and Ammon, 2002). While we were unable to determine the exact locations of source-side conversion, we assumed that conversions occurred along the azimuths to stations, i.e., to the NW or the SE (Fig. 10). In contrast to those of the North series, both *P* and *SV* waves radiated significant portions of their energies along the azimuths of stations in the South series, which may potentially explain the efficient *T* excitations. However, the *P* to *S* ratios cannot be determined unless the conversion points are known. Hence the question of whether the observed *T* waves are converted from *P* or *S* waves remains open. What is certain is that not only types of double-couple focal mechanism but also radiation patterns play a role in *T* wave excitations. This conclusion may serve as an explanation for the observation that **SF** types can be *T*-wave excited (Dziak, 2001) as long as the radiation patterns are suitable.

The *T* observations as small as M_w 5.0 from Mariana earthquakes justify our assumption that coastline stations in Taiwan and on the Ryukyu Arc islands are well positioned for *T* wave observations. Moreover, the majority of acoustic–elastic converted energies can propagate inland approximately 100 km and be recorded by stations in the Central Mountain Range. In discriminating the deficient *T* waves of tsunami earthquakes (Okal et al., 2003), the applications of Gamma were restricted to the same receiver site. In the present study, given the similar source parameters of *T*-excited earthquakes, we applied Gamma to assess the relative efficiencies of receiver-side conversions at various stations. The validity of the assessments is demonstrated by the substantial discrepancy in average Gamma between groups. To demonstrate that minor slope differences (between ~2° and ~10°) (Fig. 5) in offshore bathymetry are attributable to substantial variations of Gamma, we demonstrated that the angles of incident rays relative

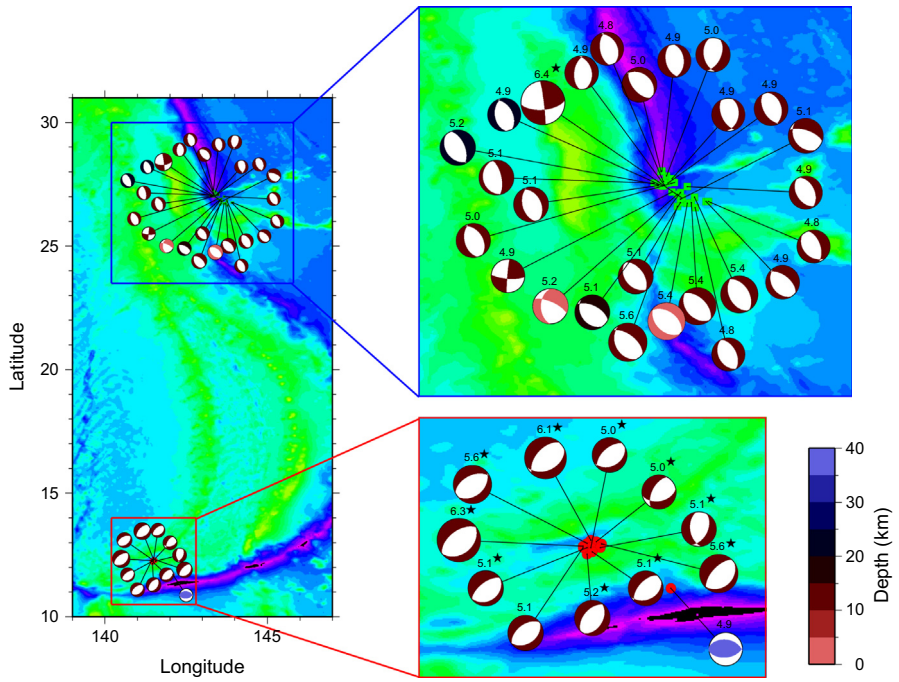

Fig. 9. Distributions and GCMT focal mechanisms (with depths color-keyed) of the two earthquake series on the north and south ends of the Mariana Arc (left). Enlarged maps for each cluster (right) show M_w on top of focal mechanisms; asterisks indicate *T*-excited events. Note the similarities of focal mechanisms within each cluster and the stark contrast of *T*-wave excitations between the North and South series. (For interpretation of the references to colour in this figure legend, the reader is referred to the web version of this article.)

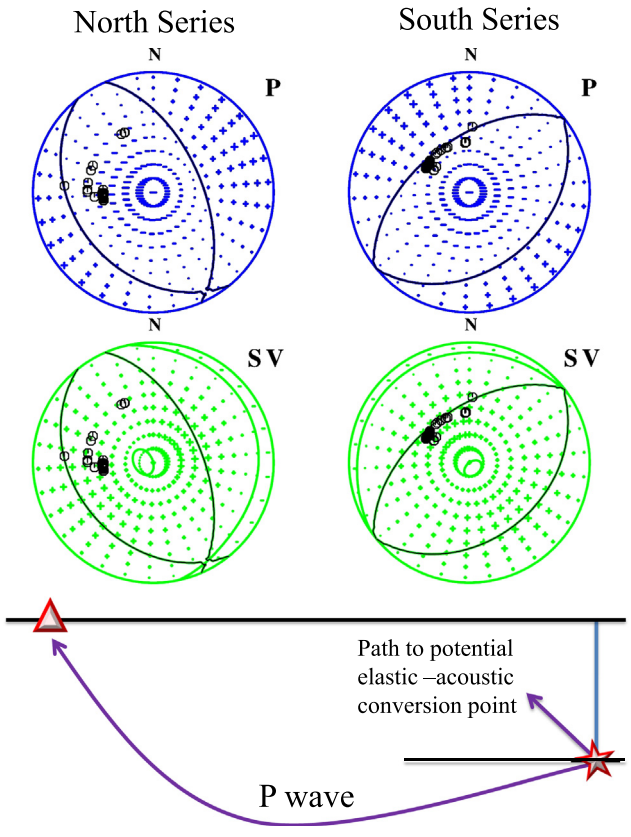

Fig. 10. (Top) lower-hemispherical projected radiation patterns with compression (+) and dilatation (−) quadrants of *P*-wave first motion by typical focal mechanisms for the North and South series. Symbol sizes are proportional to the amplitudes of *P*. Projections of rays to observing stations are shown in circles. (Middle) the same as Top but for *SV*-wave radiation patterns. (Bottom) the different ray paths for first *P* and that to the potential conversion point.

to the seafloor (θ), as measured from the normal of the seafloor, experienced a reduction of two slopes (2α) for each bounce back from the sea surface (Fig. 11), the opposite of source-side seismic rays (Johnson et al., 1963). For significant transmission (large transmission coefficients) of incident energy from medium one to medium two, the incident angles (θ) need to be smaller than the critical angle (Shearer, 2009), which can be achieved by multiple bounces between the seafloor and sea surface (Fig. 11). Assuming acoustic velocities of 1.5 km/s for oceans and 5.0 km/s for continents, the critical angle of ocean-continent incidence is about 17°. We simulated the evolutions of incident angles and water depths for three slopes (2°, 5°, and 10°) with initial incident angles in the range between 60° and 90°, and initial water depth at 1200 m (Fig. 12). Since the reductions of incident angles for each up-and-down bounce are 4°, 10°, 20° for 2°, 5°, 10° slopes, respectively, the numbers of bounces for incident angles to be less than the critical angle are greater than ten, between five and ten, and less than five, respectively (Fig. 12). We thus attribute the relatively low Gamma of Group 3 stations to their relatively small slopes (~2°) (Fig. 5) and conclude that differential slopes certainly play a primary role in controlling efficiency of receiver-side conversions.

As a final remark, although only earthquake data from 2005 were analyzed, the results may be considered representative. A preliminary examination of focal mechanisms from the entire time span of the GCMT catalogue reveals the same pattern, i.e., **TF**-type interplate earthquakes are dominant in the Izu-Bonin trench, whereas **NF**-type back-arc spreading earthquakes prevail in the Mariana trench. The excitations of *T* waves for **NF**-type earthquakes in the southern termination of the Mariana trench are so robustly observed in this study, including the 2010 South Series, that extrapolation to other time periods is relatively straightforward. Findings of consistent *T*-excited earthquakes provide opportunities for related studies, such as the observability of *T* by OBS and the seasonal and secular variations of acoustic velocities in the context of global warming (Munk et al., 1994).

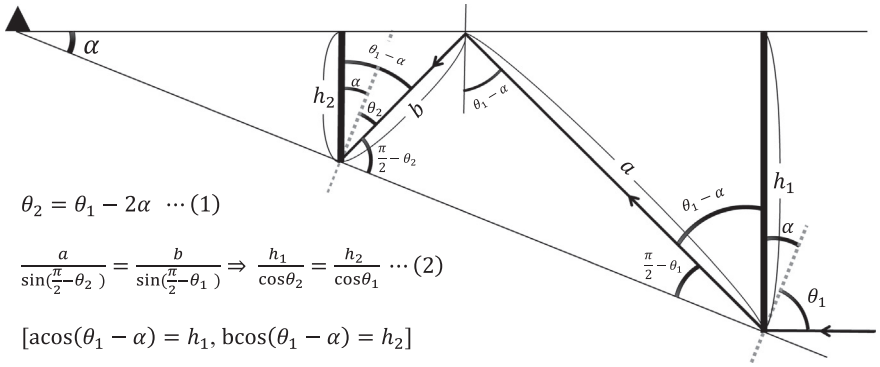

Fig. 11. Schematic illustration of changing angles (Eq. (1)) and water depths (Eq. (2)) of incidence after one upwards and downwards bounce; α: seafloor slope; θ_n: incident angle of nth incidence as measured from the normal (dashed lines) of the seafloor; h_n: water depths of nth incidence.

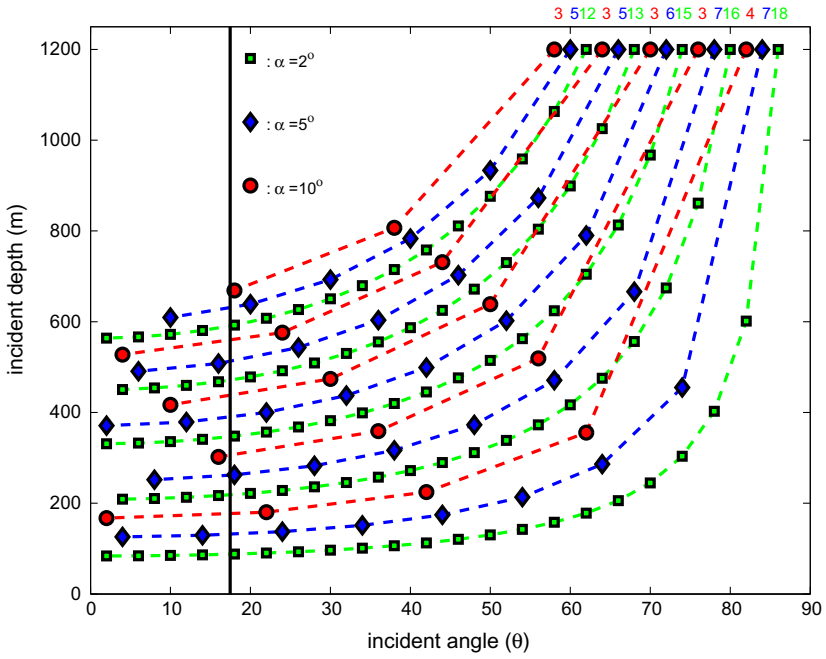

Fig. 12. Evolutions of incident angles and water depths for different seafloor slopes. Green squares, blue diamonds, and red circles represent slopes of 2°, 5°, and 10°, respectively, initiated at 1200 m water depth and various incident angles (top most symbols). The vertical solid line indicates the position of critical angle. Symbols to the left along the dashed line represent angle and water depth of next incidence based on equations of Fig. 11. Numbers on top of initiated points indicate number of bounces necessary to achieve incident angles less than critical angle. (For interpretation of the references to colour in this figure legend, the reader is referred to the web version of this article.)

5. Conclusions

Shallow earthquakes are common in the South Mariana Arc and frequently excite *T* waves as observed by stations on the Eastern Taiwan coast and on the Ryukyu Arc islands. We attribute the efficient excitation of these waves to the strong concave isobath curvature and the preferable radiation pattern of earthquakes in the vicinity of the South Mariana Arc. On the receiver side, steeply sloping offshore bathymetry plays a primary role and near perpendicular BAI angles a secondary role in contributing to efficient acoustic–elastic conversions. Findings of consistently *T*-excited earthquakes in this study provide opportunities for related studies, such as the observability of *T* by OBS and the seasonal and secular variations in acoustic velocities.

Acknowledgements

We thank NIED F-net center for providing data. This work was supported by the Taiwan Earthquake Research Center (TEC) funded through National Science Council (NSC) with Grant Number 100-2116-M-008-011. The TEC contribution number for this article is 00109. Several of the figures were prepared with the Generic Mapping Tool (GMT) software (Wessel and Smith, 1998).

References

Boatwright, J., Choy, G.L., 1986. Teleseismic estimates of the energy radiated by shallow earthquakes. J. Geophys. Res. 91, 2095–2112.
Chen, P.-F., Bina, C.R., Okal, E.A., 2004. A global survey of stress orientations in subducting slabs as revealed by intermediate-depth earthquakes. Geophys. J. Int. 159, 721–733.
deGroot-Hedlin, C.D., Orcutt, J.A., 1999. Synthesis of earthquake-generated T waves. Geophys. Res. Lett. 26, 1227–1230.
Duennebier, F.K., Johnson, R.H., 1967. T-phase Sources and Earthquake Epicenters in the Pacific Basin, Hawaii Institute Geophysics Report, 67-24. University of Hawaii, Honolulu, 104pp.
Dziak, R.P., 2001. Empirical relationship of T-wave energy and fault parameters of Northeast Pacific ocean earthquakes. Geophys. Res. Lett. 28, 2537–2540.
Dziewonski, A.M., Chou, T.-A., Woodhouse, J.H., 1981. Determination of earthquake source parameters from waveform data for studies of global and regional seismicity. J. Geophys. Res. 86, 2825–2852.

Ekström, G., Dziewonski, A.M., Maternovskaya, N.N., Nettles, M., 2005. Global seismicity of 2003: centroid-moment-tensor solutions for 1087 earthquakes. Phys. Earth Planet. Inter. 148 (1–2), 327–351, http://www.globalcmt.org.

Ewing, W.M., Woollard, G.P., Vine, A.C., Worzel, J.L., 1946. Recent results in submarine geophysics. Geol. Soc. Am. Bull. 57, 909–934.

Frohlich, C., Apperson, K.D., 1992. Earthquake focal mechanisms, moment tensors, and the consistency of seismic activity near plate boundaries. Tectonics 11, 279–296.

Herrmann, R.B., Ammon, C.J., 2002. Computer Programs in Seismology: Surface Waves, Receiver Functions and Crustal Structure. St. Louis University, St. Louis, MO. <http://www.eas.slu.edu/People/RBHerrmann/ComputerPrograms.html>.

Huang, B.-S., Chen, P.-F., Huang, Y.-L., Huang, W.-G., Liu, C.-C., 2011. Investigation of T-wave propagation in the offshore area east of Taiwan from early analog seismic network observations. Terrestrial Atmospheric and Oceanic Sciences TAO 22, 383–391. http://dx.doi.org/10.3319/TAO.2011.03.09.01(T).

Johnson, R.H., Northrop, J., Eppley, R., 1963. Sources of Pacific T phases. J. Geophys. Res. 68, 4251–4260.

Kao, H., Jian, P.R., Ma, K.F., Huang, B.S., Liu, C.C., 1998. Moment-tensor inversion for offshore earthquakes east of Taiwan and their implications to regional collision. Geophys. Res. Lett. 25, 3618–3622.

Kosuga, M., 2011. Localization of T-wave energy on land revealed by a dense seismic network in Japan. Geophys. J. Int. 187, 338–354. http://dx.doi.org/10.1111/j.1365-245X.2011.05143.x.

Lin, C.H., 2001. T-wave excited by S-wave and oscillated within the ocean above the southeastern Taiwan forearc. Geophys. Res. Lett. 28, 3297–3300. http://dx.doi.org/10.1029/2001GL013152.

Linehan, D.S.J., 1940. Earthquakes in the West Indian region. Trans. Am. Geophys. Union 21, 229–232.

Munk, W.H., Spindel, R.C., Baggeroer, A., Birdsall, T.G., 1994. The Heard Island feasibility test. J. Acoust. Soc. Am. 96, 2330–2342.

Obara, K., Maeda, T., 2009. Reverse propagation of T waves from the Emperor seamount chain. Geophys. Res. Lett. 36, L08304. http://dx.doi.org/10.1029/2009GL037454.

Okal, E.A., Talandier, J., 1997. T waves from the great 1994 Bolivian deep earthquake in relation to channeling of S wave energy up the slab. J. Geophys. Res. 102, 27,421–27,437.

Okal, E.A., Alasset, P.-J., Hyvernaud, O., Schindelé, F., 2003. The deficient T waves of tsunami earthquakes. Geophys. J. Int. 152, 416–432.

Okal, E.A., 2001. "Detached" deep earthquakes: are they really? Phys. Earth Planet. Inter. 127, 109–143.

Okal, E.A., 2008. The generation of T waves by earthquakes. Adv. Geophys. 49, 1–65.

Park, M., Odom, R.I., Soukup, D.J., 2001. Model scattering: a key to understanding oceanic T-waves. Geophys. Res. Lett. 28 (17), 3401–3404.

Shearer, P.M., 2009. Introduction to Seismology. Cambridge University Press, Cambridge.

Talandier, J., Okal, E.A., 1998. On the mechanism of conversion of seismic waves to and from T waves in the vicinity of island shores. Bull. Seismol. Soc. Am. 88, 621–632.

Talandier, J., Okal, E.A., 2001. Identification criteria for sources of T waves recorded in French Polynesia. Pure Appl. Geophys. 158, 567–603.

Walker, D.A., 1989. Seismicity of the interiors of plates in the Pacific Basin. Eos, Trans. Am. Geophys. Union 70, 1543-1533.

Wessel, P., Smith, W.H.F., 1998. New, improved version of the Generic Mapping Tools Released. Eos, Trans. Am. Geophys. Union 79, 579.